Continuous Transitions between Levels of Autonomy based on Virtual Fixtures for Surgical Robotic Systems

Katharina Hagmann[1], Anja Hellings-Kuß[1], Florian Steidle[1], Freek Stulp[1], Daniel Leidner[1], Julian Klodmann[1]

***Abstract*— Nowadays, telemanipulation robotic systems are present in many operating rooms. The exploitation of autonomy for minimally invasive robotic surgery remains an open field of research as it is non-trivial to provide meaningful assistance. This work presents a novel virtual fixture providing haptic augmentation for shared control as well as task-level autonomy, while ensuring continuous transitions of control between the robotic system and the surgeon. Transitions between levels of autonomy are based on information about the robotic system and its environment. The proposed method is evaluated through experiments which show the successful completion of surgeon training tasks, namely peg transfer and suturing, exploiting shared control and task-level autonomy.**

I. Introduction

Minimally invasive robotic surgery (MIRS) is widespread and established in operating rooms. It provides similar advantages to patients as minimally invasive surgery, i.e. shorter recovery time and minimal scarring due to small incisions. At the same time MIRS offers surgeons improved ergonomics and a restored hand-eye coordination. Commercially available surgical robots for MIRS are telemanipulation systems. They act as the surgeon's hands and eyes inside the patient's body. This means the surgeon directly controls the movement of the telemanipulation system in all available, mostly six, *Degrees of Freedom* (DoF).

Recent scientific approaches aim at increasing the autonomy of telemanipulation systems. *Levels of Autonomy* (LoA) classify both the generation and selection of a surgical plan as well as this plan's execution and monitoring. They range from *no autonomy* (L0) over *robot assistance* (L1), *task-level autonomy* (L2), *supervised autonomy* (L3) and *high-level autonomy* (L4) towards *full autonomy* (L5) [1],[2],[3],[4]. This work focuses on the following LoA:

- L0: The surgeon can freely telemanipulate the instrument tip within its inherent workspace.
- L1: The robotic system assists the user with shared control based on haptic augmentation.
- L2: The robotic system controls all DoF to fulfill a previously defined task.

To this end, this work contributes with a novel interactive task-level autonomy based on *Virtual Fixtures* (VF) enabling the user to fine-tune autonomous motions by interacting with the input device. We introduce a novel *interactive feed forward Virtual Fixture* (iffVF) extending well known *attractive Virtual Fixtures* (aVF). The iffVF offers not only autonomous motions during L2 but also shared control during L1. Additionally, the iffVF allows the continuous adaption of the support i.e. the *Degree of Shared Control* DoSC in L1. DoSC enables the surgeons to fine tune the provided support according to their needs.

Surgery causes dynamically changing environments and, thus, requires continuous and fast transitions of control, in particular, from the robotic system (L2) to the surgeon (L1 or L0) at all times [4],[5]. To facilitate these transitions we propose the *Autonomy and Shared Control Parameterization Engine* (ASCOPE). ASCOPE determines the LoA chosen by the user and adjusts the parameters of the iffVF accordingly based on context information of the robotic system, its environment and the current state of a task.

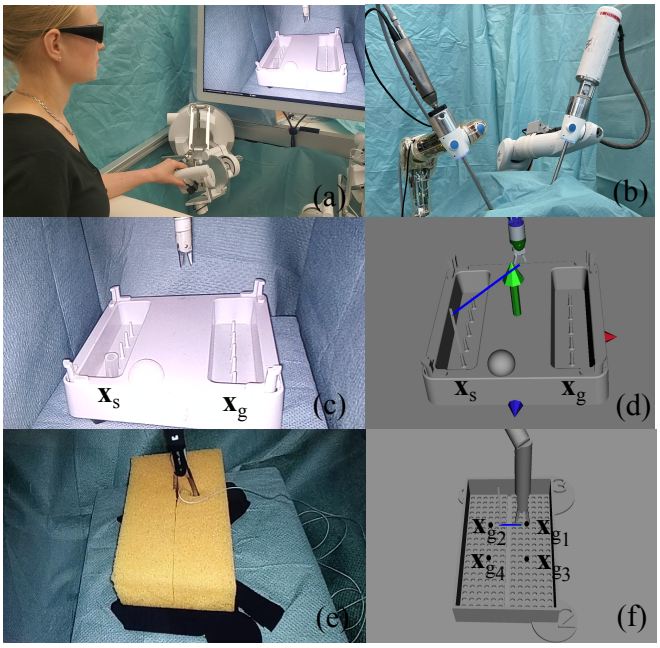

Fig. 1: The DLR MiroSurge system consists of a surgeon console (a) and MIRO robotic arms holding a surgical instrument and the endoscope (b). (c) depicts the peg transfer task performed in Section IV-C. (d) shows the digital twin with task specific splines. (e) depicts the suturing task performed in Section IV-D, while (f) shows the corresponding digital twin.

[1] German Aerospace Center (DLR), Robotics and Mechatronics Center (RMC), Münchner Str. 20, 82234 Weßling, Germany, corresponding author: katharina.hagmann@dlr.de

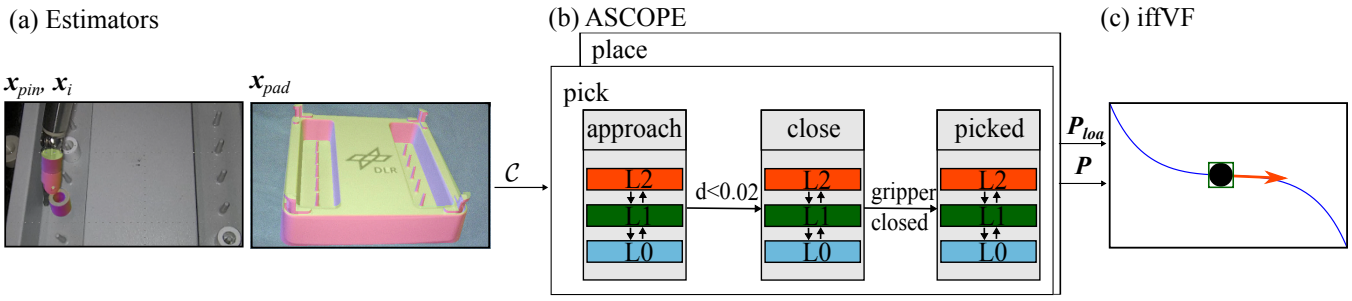

Fig. 2: Estimators as in [5] provide context information $\mathcal{C}$. ASCOPE determines the current state of the task and the selected LoA accordingly and selects the parameters $\boldsymbol{P}$ and the LoA specific parameters $\boldsymbol{P}_{loa}$ to parameterize VFs. The iffVF allows user interactions even in L2. The `pick` task serves as an example for an arbitrary task.

The main contributions of this work are

- the presentation of ASCOPE allowing the adaption of LoA and the parameterization of the novel iffVF based on the selected LoA and the current state of the task
- the introduction of iffVF enabling interactive task-level autonomy by a feed forward wrench and smooth transitions between all presented LoA
- the adaption of the degree of shared control during L1.

After discussing the state of the art in comparison to the contribution of this paper in Section II, Section III provides detailed insights into the proposed methods. In Section IV we evaluate the technical feasibility of the presented methods. Section V discusses the proposed methods and presents an outlook.

II. State of the Art

This section gives an overview of related works. The first part focuses on L2 and L1, while the second part discusses transitions between different LoA.

Several works introduce L2 for a surgical peg transfer and compare the results of the autonomous execution to human performance using a telemanipulation setting [6],[7],[8]. In [9],[10],[11] approaches are introduced to autonomously place sutures. Kam *et al.* present a method for suturing on synthetic vaginal cuff tissues [12]. The suture execution is performed autonomously. Saedi *et al.* execute an autonomous intestinal anastomosis with the STAR system [13]. These works present systems for L2 without focusing on transitions to L1 or L0. User interactions with a haptic input device are not possible during L2.

Regarding L1, telemanipulation can be assisted by automated scaling of the user input [14] or VFs enabling haptic augmentation [15], [16], [17]. rVFs protect the user from entering a prohibited zone. Geometric primitives, as well as meshes [18] and visual servoing information [19] can determine the shape of a VF. In [20] uncertainties of visual pose detection are used to parameterize a visual servoing VF. aVFs haptically guide a user towards a goal structure. In [21] the user is able to generate aVFs and adapt their geometry and position by a human-in-the-loop approach. These works offer support in L1 without the option of switching to L2.

Fontanelli *et al.* design a state machine for needle insertion and extraction [22]. Transitions are triggered by predefined user gestures. The LoA, i.e. L0, L1 or L2, is pre-selected and not changed during the execution of a task.

Some works discuss transitions between different LoA. In [23], a confidence-based supervised-autonomous control strategy shifts the control between the user in telemanipulation and an autonomy module applying a joint space interpolator. Ferraguti *et al.* ensure a fast and stable switch from L2 to L0 by compensating the pose offset between leader and follower [24]. Shamaei *et al.* introduce a dominance factor which allows the continuous switching of authority between an arbitrary autonomous agent and the telemanipulation by a user. Additionally, an aggressiveness factor sets the allowed pace of the autonomous agent [25]. In [26] the robotic system allocates autonomously the authority among the human operator and itself. In [27] the user authorizes the switch from L1 to L2 by pressing a button but not vice versa. These works ensure switching either between L2 and L0 or between L1 and L2.

To the authors knowledge no methods exist comprehensively addressing L0, L1 and L2 as well as transitions between all presented LoA for MIRS systems.

III. Methods

The methods explained in this section are exemplified on a pick task of the peg transfer with a surgical instrument. Section III-A describes the details of the ASCOPE, which is depicted in Fig. 2b. The novel iffVF is introduced in Section III-B and graphically shown in Fig. 2c.

A. Autonomy and Shared Control Parameterization Engine

Depending on the LoA selected by the user, ASCOPE parameterizes the iffVF according to the context information $\mathcal{C}$ about the robot and the environment, depicted in Fig. 2 (a), as well as the progress of the task. A task defines the interaction of a reference object O_{ref} with a target object O_{tar}. In the `pick` a ring example, the ring serves as O_{tar} and the surgical instrument as O_{ref}. A task is composed of different sub-tasks. *Shared Control Templates* (SCTs), introduced in [28], model the different sub-tasks as states of a state machine. Fig. 2b depicts the `pick` SCT, with the states 'approach' and 'close'. 'picked' is the goal state $state_g$.

Conditions based on wrenches $\boldsymbol{w}$, poses $\boldsymbol{x}$ and distances

$d \in \mathbb{R}$ between O_{ref} and O_{tar} allow transitioning from one state to another. A wrench $\boldsymbol{w} = [\boldsymbol{f}; \boldsymbol{\tau}] \in \mathbb{R}^6$ is composed of forces $\boldsymbol{f} \in \mathbb{R}^3$ and torques $\boldsymbol{\tau} \in \mathbb{R}^3$. Pose $\boldsymbol{x}$ refers to the rotation $\boldsymbol{R} \in \mathbb{R}^{3\times3}$ and position $\boldsymbol{p} \in \mathbb{R}^{3\times1}$ of a homogeneous transformation matrix $\boldsymbol{T} \in SE(3)$.

In [29] we present SCOPE, extending SCTs. SCOPE encodes a set of parameters $\boldsymbol{P}$ in each state, which are used to parameterize VFs for L1 depending on the current state of the task. ASCOPE adds the definition of LoA specific parameters $\boldsymbol{P}_{loa}$ to each state. This allows not only the parameterization of VFs according to the current state of the task but also depending on the chosen LoA. Algorithm 1 describes ASCOPE. The execution starts at

Algorithm 1: Pseudocode of the ASCOPE main loop to parse SCTs, query the selected LoA and parameterize VFs. * mark the extensions form SCOPE to ASCOPE.

Input: The SCT encoding the current task.

Output: The algorithm terminates nominal as all states of the SCT are processed.

```
state_cu ← 0
state_g ← getGoal(SCT)
O_ref, O_tar ← getReferenceAndTarget(SCT)
while state_cu ≠ state_g do
    C ← getContextInformation(O_ref, O_tar)
    state_cu ← getCurrentState(C, SCT, state_cu)
    P ← getParameter(state_cu)
    loa_id ← getCurrentLoA() *
    P_loa ← getParameter(state_cu, loa_id, SCT)*
    parametrizeVF(P,P_loa)
return True
```

the first state defined in the SCT and stops when reaching the goal state $state_g$ acquired from the SCT by `getGoal`. `getReferenceandTarget` determines O_{ref} and O_{tar} based on the current task. The estimators provide the function `getContextInformation` retrieving $\mathcal{C}$ based on O_{ref} and O_{tar}. This allows the determination of the current state $state_{cu}$ by `getCurrentState` ensuring possible transitions to subsequent states. According to $state_{cu}$ the SCT offers the corresponding $\boldsymbol{P}$ using `getParameter`. As extension to the formerly presented SCOPE, ASCOPE introduces the function `getCurrentLoA` querying the selected LoA . `getParameter` retrieves $\boldsymbol{P}_{loa}$ from the SCT based on $state_{cu}$ and loa_{id}. $\boldsymbol{P}_{loa}$ and $\boldsymbol{P}$ update the corresponding VFs by `parameterizeVF`.

B. Interactive feed forward VF covering L2, L1 and L0

VFs implement a virtual *Spring-Damper System* (SDS) between the instrument TCP $\boldsymbol{x}$ and a virtual proxy. The deflection of the SDS generates virtual wrenches $\boldsymbol{w}$. In a telemanipulation setup, they can be projected to haptic input devices. aVF haptically guides the user to align e.g. the pose of the instrument TCP with a desired pose.

In [29] a cylindrically shaped *path following aVF* (paVF), as depicted in Fig. 3a, is proposed along a generated spline s. Its pose $\boldsymbol{x}_a$ is always located on s and the longitudinal axis oriented along s. The radius r and the length l act as translational deadzones. α defines a rotational deadzone acting on the angular deviation between the orientation of $\boldsymbol{x}_a$ and $\boldsymbol{x}$. $\boldsymbol{x}$ moves freely inside the deadzones. If a wrench $\boldsymbol{w}_e$ (e.g. user input at the haptic input device), leads $\boldsymbol{x}$ to leave the cylinder the virtual proxy, with pose $\boldsymbol{x}_p$, stays on the cylinder wall. The SDS between $\boldsymbol{x}_p$ and $\boldsymbol{x}$ is deflected causing $\boldsymbol{w}$, which acts on $\boldsymbol{x}$ and is projected to the haptic input device. $\boldsymbol{w}_a = [\boldsymbol{f}_a, \boldsymbol{\tau}_a]$ acts on $\boldsymbol{x}_p$ and has the same magnitude as $\boldsymbol{w}$ but opposite direction.

This work extends the paVF with a feed forward behavior to encode different LoA while allowing user interactions and, therefore, presents the novel iffVF. Splines are used to represent the task at hand. The following paragraphs describe the presented iffVF for L2 in Section III-B.1, L1 in Section III-B.2 and L0 in Section III-B.3. transitions are explained in Section III-C. Table I gives an overview of $\boldsymbol{P}_{loa}$, which are introduced in this section.

1) L2 - task-level autonomy: L2 requires precise autonomous guidance along an arbitrary spline. The novel iffVF ensures this guidance and enables user interactions during L2 for fine corrections. Precision is enforced by $\boldsymbol{x}_p = \boldsymbol{x}_a$. Therefore, the deadzones $r = l = \alpha = 0$ enclose the virtual proxy at $\boldsymbol{x}_a$, with position $\boldsymbol{p}_a$. For autonomous guidance along an arbitrary spline s, $\boldsymbol{x}_a$ has to move along s as shown in Fig. 3b. Therefore, the iffVF is extended by a virtual mass point with mass M and damping factor D at $\boldsymbol{x}_a$. It follows the equation of motion

$$M\ddot{\boldsymbol{p}}_a + D\dot{\boldsymbol{p}}_a = f_f^{\parallel}. \tag{1}$$

$f_f^{\parallel}$ contains a definable constant force $f_c^{\parallel}$ along s causing a continuous movement of $\boldsymbol{x}_a = \boldsymbol{x}_p$. As $\boldsymbol{x}_p$ is connected to $\boldsymbol{x}$ by an SDS this leads to autonomous guidance of $\boldsymbol{x}$.

Enabling user interaction during L2 is a core feature of iffVF. $\boldsymbol{f}_e$ is the sum of user forces on the input device and resisting forces, e.g. resulting from other VFs, like rVFs, friction or damping. $\boldsymbol{f}_e$ acts on $\boldsymbol{x}$. It causes the deflection of the SDS between $\boldsymbol{x}$ and $\boldsymbol{x}_p$ resulting in $\boldsymbol{f}_a$ acting on $\boldsymbol{x}_a$. $f_a^{\parallel}$ is the component of $\boldsymbol{f}_a$ along s. Finally, $f_f^{\parallel}$ results in

$$f_f^{\parallel} = f_c^{\parallel} + f_a^{\parallel}. \tag{2}$$

ensuring that the user can interact with the iffVF by accelerating or decelerating it, and its compliance with other VFs.

2) L1 - robot assistance: In L1, the robot assists the user by means of shared control. The user controls the movement of $\boldsymbol{x}$ along the spline and receives haptic augmentation in the remaining DoFs to stay on the trajectory. $f_c^{\parallel}$ is set to 0. DoSC describes a continuous scale of support. High support ensures very precise guidance on s by setting a small desired radial deadzone r_d and a small desired rotational

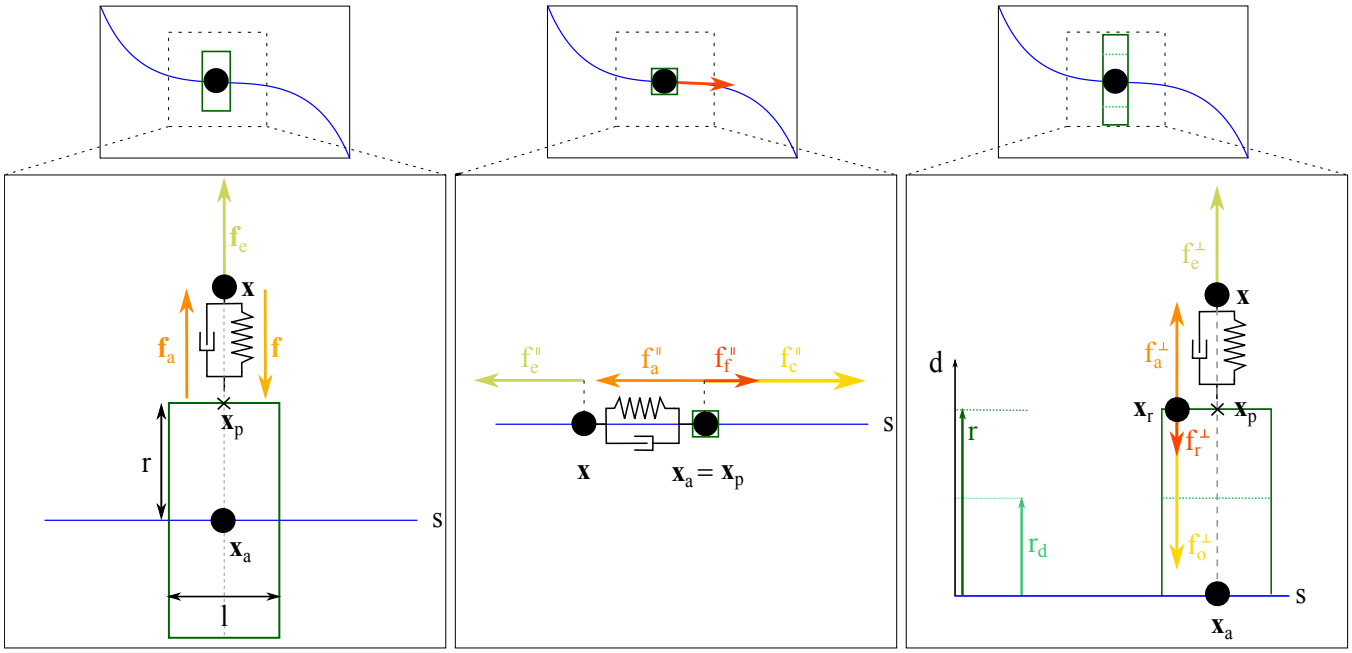

(a) $\boldsymbol{x}_p$ stays on the cylinder wall if $\boldsymbol{f}_e$ causes $\boldsymbol{x}$ to leave the cylinder generating $\boldsymbol{f}$ and $\boldsymbol{f}_a$. r and l determine the length and radius of the cylinder.

(b) In L2, $r = l = 0$ results in $\boldsymbol{x}_a = \boldsymbol{x}_p$. $f_f^{\parallel}$, which is influenced by $f_e^{\parallel}$ through $f_a^{\parallel}$, acts on $\boldsymbol{x}_a$ causing its movement.

(c) In L1, DoSC determines r_d. If $r_d \neq r$, $f_r^{\perp}$ acts on a damped mass point at $\boldsymbol{x}_r$ causing r to decrease. $\boldsymbol{x}_p$ stays on r.

Fig. 3: An iffVF at $\boldsymbol{x}_a$ on s is presented in (a) and adapted for L2 in (b) and L1 in (c). r and l are depicted in green. s is shown in blue. $\boldsymbol{f}_e$ (light green) combines the sum of user forces on the input device and other counteracting forces, i.e. VF and other dynamic effects of the input device, such as inertia and friction. $\boldsymbol{f}_e$ deflects the SDS between $\boldsymbol{x}_p$ and $\boldsymbol{x}$. This generates a force $\boldsymbol{f}$ causing $\boldsymbol{x}$ to follow $\boldsymbol{x}_p$. Black circles depict mass points.

deadzone α_d. Low support keeps $\boldsymbol{x}$ inside a region of interest, parameterized by a greater r_d and α_d, while the user fine-manipulates. Therefore, the DoSC is continuously adapted by varying r_d and α_d.

In this work, we introduce the parameter $k_r \in [0; 1]$ to vary the DoSC according to the user's selection.

$$r_d = k_r r_{d,max}, \tag{3}$$

defines the mapping between r_d, the selected k_r and $r_{d,max}$, the maximal allowed radius predefined by the minimal required task precision.

If r_d varies, the current radius r should follow this variation. To this end, an analog method as in Section III-B.1 is chosen. A force $f_r^{\perp}$, orthogonal to s, allows a smooth and continuous variation of r. A virtual mass point with mass M_r and damping factor D_r is introduced, whose position represents r. The point follows

$$M_r \ddot{r} + D_r \dot{r} = f_r^{\perp}. \tag{4}$$

If $f_r^{\perp}$ contains a definable constant force $f_o^{\perp}$, this allows the decrease and increase of r by

$$f_o^{\perp} \begin{cases} > 0 & \text{if } r > r_d \\ = 0 & \text{if } r = r_d \\ < 0 & \text{if } r < r_d \end{cases} \tag{5}$$

User interactions and compliance to other VFs should be ensured in the variation of r. The force the user applies on the input device and resisting forces, e.g. resulting from other VFs, like rVFs, friction or damping, are entailed in $\boldsymbol{f}_e$, which acts on $\boldsymbol{x}$. It causes the deflection of the SDS between $\boldsymbol{x}$ and $\boldsymbol{x}_p$ resulting in $\boldsymbol{f}_a$ acting on $\boldsymbol{x}_a$, with $f_a^{\perp}$ its component orthogonal to s. Finally, $f_r^{\perp}$ results in

$$f_r^{\perp} = \begin{cases} f_o^{\perp} + f_a^{\perp} & \text{if } r \neq r_d \\ 0 & \text{otherwise.} \end{cases} \tag{6}$$

If $r = r_d$ applies, $f_r^{\perp}$ is set to 0 to ensure the desired haptic guidance. The decrease of r is depicted in Fig. 3c. The same method is applied for α_d.

If the user moves the input device along s this results in $f_a^{\parallel}$ acting on $\boldsymbol{x}_a$, as $l = 0$. Following Eq. (1) and Eq. (2) the position of iffVF, $\boldsymbol{p}_a$, moves accordingly.

3) L0 - no autonomy: During L0 the user can telemanipulate the instrument TCP freely within its workspace because $f_c^{\parallel} = 0$ and $f_o^{\perp} = 0$. During L1, $f_r^{\perp}$ is set to $f_a^{\perp}$, so the virtual mass point located on r moves when $\boldsymbol{x}$ moves orthogonal to s, constantly increasing or decreasing the corresponding deadzone. As $\boldsymbol{x}$ always stays inside the cylinder, the user receives telemanipulation without haptic augmentation. l is set to 0, which causes an updated movement of $\boldsymbol{p}_a$ as explained in the previous paragraph. The continuous update of $r = r_d$, $\alpha\alpha_d$ as well as $\boldsymbol{p}_a$ enables

the continuous switching to L1 and L2 as explained in the following section.

C. Transitions between LoA

$\boldsymbol{P}_{loa}$ for distinct LoA				
Type	L0	L1	L2	Description
$f_c^{\parallel}$	0	0	>0	force along s
$f_o^{\perp}$	0	Eq. (6)	0	force orthogonal to s
r	>0	r_d	0	radial deadzone
α	>0	α_d	0	rotational deadzone
l	0	0	0	axial deadzone

TABLE I: This table gives an overview of required $\boldsymbol{P}_{loa}$ which are described in detail in Section III-B .

The presented iffVF encodes L0, L1 and L2 with $\boldsymbol{P}_{loa}$ consisting of $f_f^{\parallel}$, r_d, α_d and l. Variation of $f_c^{\parallel}$, r_d and α_d allows the transitions between different LoA. Table I gives an overview of these parameters for the different LoA.
For transitions from L0 to L1, α_d and r_d are set according to the current DoSC as described in Eq. (3). While $\alpha_d \neq \alpha$ or $r_d \neq r$, the corresponding deadzone is extended or decreased as explained in Section III-B.2. This ensures as much guidance for the user as selected by the DoSC. The switch from L1 to L0 is enabled by continuously adapting α_d and r_d to $\boldsymbol{x}$, and thus also r and α, so $\boldsymbol{x}$ stays inside the cylindrical VF.
For a hand-over from L1 to L2 minimal deadzones are required resulting in $r_d = \alpha_d = 0$. r_d and α_d are decreased by applying $f_r^{\perp}$ according to Eq. (4). $f_c^{\parallel} > 0N$ leads to a gradually increased acceleration of $\boldsymbol{x}_a$ resulting in an autonomous motion of $\boldsymbol{x}$ along s. For the transition from L2 to L1 $f_c^{\parallel} = 0N$ results in no autonomous motion of $\boldsymbol{x}_a$ anymore. r_d and α_d are adapted according to the current DoSC. In general, the user overseeing and controlling the robotic system needs to acknowledge a change from a lower to a higher LoA and vise versa.

IV. Evaluation

This section presents experiments which evaluate the proposed methods. They are conducted on the DLR MiroSurge surgical robotic research platform depicted in Fig. 1. A 7-DoF light weight robotic arm MIRO is mounted on the side rail of an OR table. A drive unit is attached to the MIRO which actuates a wristed surgical instrument with additional 2 DoFs and a functional DoF, i.e. a grasper or a needle handover device. A Force Dimension sigma.7 [30] steers the pose of the instrument TCP $\boldsymbol{x}$. The sigma.7 is a 6 DoF input device with an additional gripping DoF. It allows the rendering of forces and torques in 7 DoF. A second MIRO carries an endoscope. A software layer uses a position controller to map the motion of up to two input devices to $\boldsymbol{x}$ and the endoscope TCP of multiple avatar robots using an inverse kinematics which preserves the motion constraints at the incision point [31],[32]. The components of the DLR MiroSurge platform communicate at a frequency of more than 1 kHz in real time.
In all experiments $M = M_r = 0.01kg$ and $D = D_r = 10\frac{Ns}{m}$ are set. The experiments described in Section IV-A and Section IV-B utilize a simulated endeffector and MIRO as described in Chapter 8 of [33]. The experiment presented in Section IV-C and Section IV-D are conducted on the real endeffectors and MIROs. All experiments utilize a sigma.7 haptic input device.

A. Interactive task-level autonomy L2

This experiment evaluates the compliant behavior of iffVF to other VFs. As example of a rVF, a cylindrical virtual wall is implemented in the workspace of $\boldsymbol{x}$ as in [29]. Reaching the virtual wall causes the counteracting virtual wrenches $\boldsymbol{w}_w = [\boldsymbol{f}_w, \boldsymbol{\tau}_w]$ which are projected to the input device. $\boldsymbol{w}_w$ influences the movement of iffVF.

Hypothesis: Before $\boldsymbol{x}$ has reached the wall, it follows $\boldsymbol{x}_p$. If $\boldsymbol{x}$ gets in contact with the virtual wall, the movement of $\boldsymbol{x}_p = \boldsymbol{x}_a$ is decelerated and finally stopped at the equilibrium of $f_a^{\parallel}$ and $f_c^{\parallel}$.

Experimental Design: An SCT with one state defining a linear spline s in Cartesian space between $\boldsymbol{p}_{ref}$, the position of O_{ref}, and $\boldsymbol{p}_{tar}$, the position of O_{tar}, is used. L2 is set during the whole experiment with $f_c^{\parallel} = 2N$. There are no user interactions with the sigma.7.

Result: Fig. 4 shows that when $\boldsymbol{x}$ reaches the virtual wall its motion decelerates. Thereby, the motion of $\boldsymbol{x}_p$ is decelerated and stops at the equilibrium of $f_a^{\parallel}$ and $f_c^{\parallel}$, i.e. $f_f^{\parallel} = 0$.

Discussion: This experiment demonstrates how iffVF achieves interactive task-level autonomy. The interactive behavior in the presence of an rVF shows that the iffVF complies with other VFs. The same approach allows user interactions as acceleration or deceleration during L2.

B. Transitions between LoA

The following experiment evaluates the transitions between L2 and L1 as well as variation in the DoSC, while $\boldsymbol{x}$ follows $\boldsymbol{x}_p$ along s.

Hypothesis: The transitions between L1 and L2 as well as variations in the DoSC lead to variations in r_d and $f_c^{\parallel}$ respectively. These transitions result in smooth trajectories of $\boldsymbol{x}$.

Experimental Design: The same SCT as presented in Section IV-A generates s. Different LoA as well as DoSC are selected according to the table in Fig. 5a. During L1 the user telemanipulates the DoF along s, while all other DoF are constraint by the iffVF. In L2 there are no user interactions with the sigma.7.

Result: Fig. 5a displays the movement of $\boldsymbol{x}$ during L1 and L2. The user experiences unconstrained movements inside the radial deadzone as well as forces and torques if $\boldsymbol{x}$ leaves the deadzone. The varying LoA and DoSC lead to variations in r_d causing an increase or decrease of r. $\boldsymbol{x}$ follows the movement of the iffVF with a smooth trajectory.

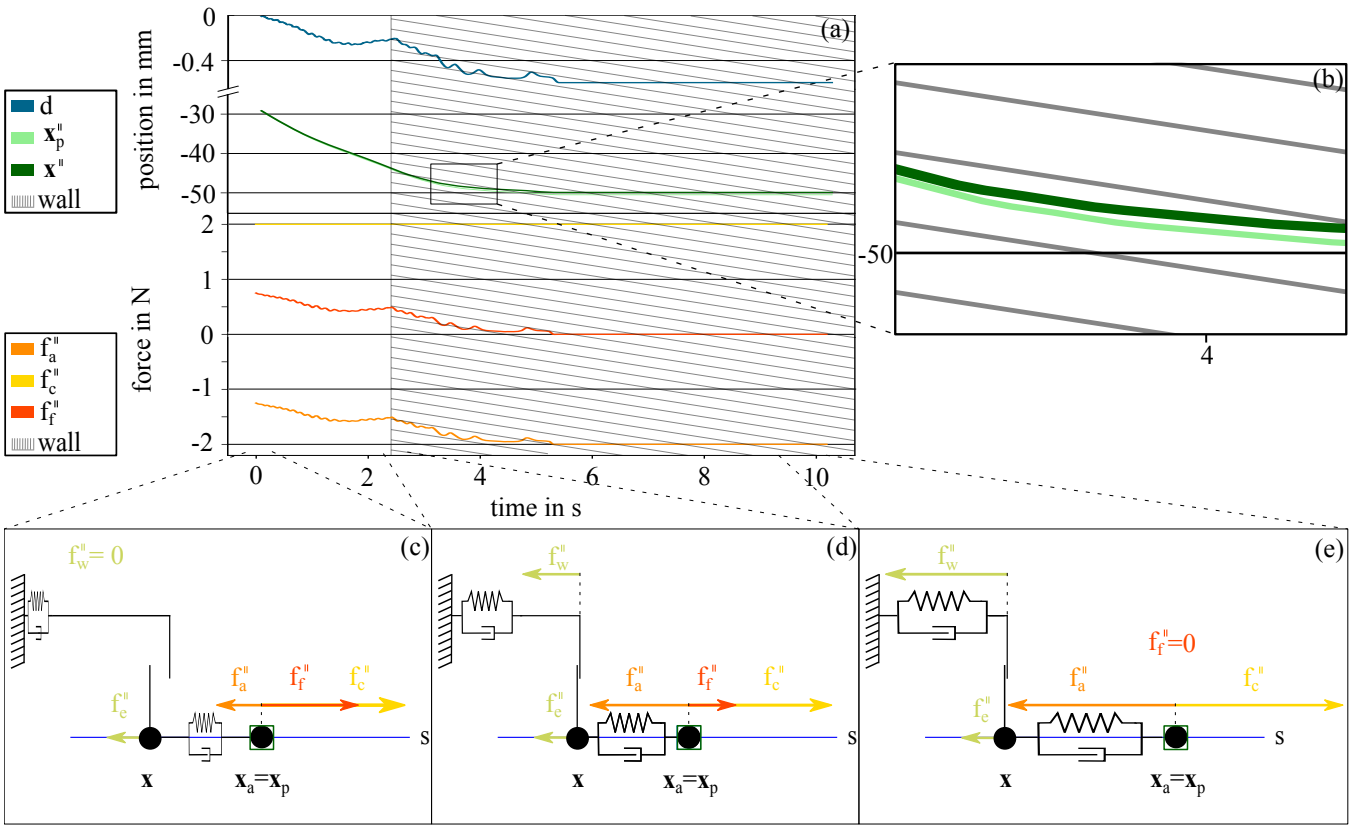

Fig. 4: (a) shows the positions of $\boldsymbol{x}^{\parallel}$ and $\boldsymbol{x}_p^{\parallel}$ in axial direction on s in green, as well as their distance d in blue. Furthermore, (a) depicts the development over time of $f_c^{\parallel}$ (yellow), $f_a^{\parallel}$ (orange) and $f_f^{\parallel}$ (dark orange). At $t = 0s$ $\boldsymbol{x}$ and $\boldsymbol{x}_p$ start moving as depicted in (c) slightly disturbed by the dynamic effects of the input device. At $t = 2.2s$ $\boldsymbol{x}$ hits the virtual wall shown in (d). As $f_w^{\parallel}$ increases, the motion of $\boldsymbol{x}$ decelerates and its distance to $\boldsymbol{x}_p$ increases (b). This increases $f_a^{\parallel}$. Accordingly, the motion of $\boldsymbol{x}_p$ is decelerated until it stops, at the equilibrium of $f_a^{\parallel}$ and $f_c^{\parallel}$, i.e. $f_f^{\parallel} = 0$ (e).

Discussion: The evaluated concept of the iffVF and AS-COPE allows transitions between the presented LoA while ensuring smooth trajectories of $\boldsymbol{x}$. If the $\boldsymbol{x}$ stays inside the cylindrical iffVF at L1, the user can manipulate without any virtual wrenches present resulting in a movement like in L0. While reaching the lateral area of the cylinder, support in form of haptic guidance is present.

C. Surgeon Training Task - Peg Transfer

Training curricula as the Lübecker Toolbox [34] allow the surgeon to acquire basic skills like instrument handling and manipulation skills. This experiment presents a peg transfer task, provided by the Lübecker Toolbox's Bantwist training pad, on the real MICA and MIROs which is depicted in Fig. 1. A video of the task execution is provided as supplementary material. The SCT `pick` (depicted in Fig. 2 b), `transition` and `place` are executed one after another. The control over the opening and closing of the gripping DoF remains by the user at all times. During the execution there are switches in the DoSC as well as the LoA.

Hypothesis: If the SCT `pick`, `transition` and `place` are executed in a sequence the ring is successfully transferred from $\boldsymbol{x}_s$ to $\boldsymbol{x}_g$, as shown in Fig. 1, exploiting transitions between L2 and L1 and vice versa, as well as varying DoSC.

Experimental Design: To achieve the peg transfer, the SCT `pick`, `transition` and `place` operate with $O_{ref} = \boldsymbol{x}$. `pick` sets $O_{tar} = \boldsymbol{x}_s$, while `transition` and `place` use $\boldsymbol{x}_g$ as O_{tar}. As soon as $state_g$ of the currently active SCT is reached, $state_0$ of the succeeding SCT is activated. During this experiment the pose of the training pad is provided by the vision-based tracker presented in [35]. The LoA as well as the DoSC are varied according to the table in Fig. 5a, resulting in a variation of r_d, while $\alpha_d = 0$ is set. In L1, the user controls the DoF along the spline and the movement inside the deadzones. During L2, the user either removes the hand from the input device or interacts with L2 to adjust the velocity of task execution.

Result: The peg is successfully picked at $\boldsymbol{x}_s$ and placed at $\boldsymbol{x}_g$. Fig. 5b depicts the movement of $\boldsymbol{x}$ and the varying r during the experiment.

Discussion: This experiment shows the combination of the experiments in Section IV-A and Section IV-B, as the user interacts with the input device in L2, leading to successful completion of a meaningful task in surgeon training.

D. Surgeon Training Task - Suturing

The skills trained by performing training tasks are required to perform surgeries as a fundoplication. It treats the reflux

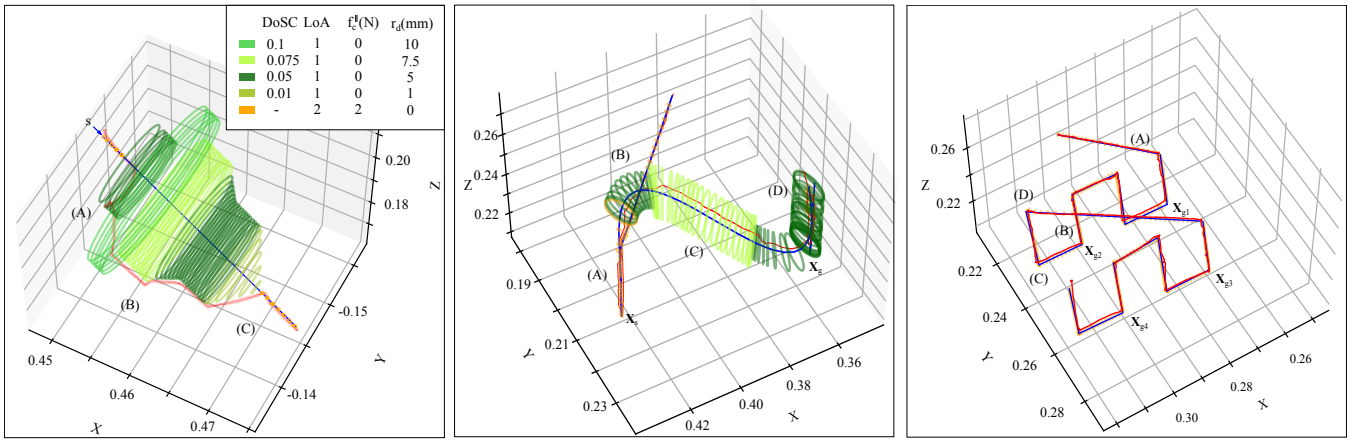

(a) (A) The hand-over from L2 to L1 causes $f_c^{\parallel} = 0N$. The user takes over and moves $\boldsymbol{x}$ freely inside the cylinder. (B) The DoSC is varied leading to a continuous adaption of r_d. The user moves along the spline while the iffVF controls the remaining Cartesian DoF. (C) L2 is selected, the user removes the hand from the input device.

(b) (A) The user selects L2, so $\boldsymbol{x}$ picks the ring autonomously at $\boldsymbol{x}_s$ with $f_c^{\parallel} = 2N$ using the `pick` SCT. (B) The user switches to L1 and moves the sigma along the spline while experiencing haptic augmentation in the remaining DoFs. (C) The DoSC is modulated according to the legend in Fig. 5a. (D) The ring is placed at $\boldsymbol{x}_g$ in L1.

(c) The user selects L2 throughout the experiment resulting in $f_c^{\parallel} = 2N$. (A) $\boldsymbol{x}$ approaches $\boldsymbol{x}_{g1}$ using the `suture` SCT. (B) The user closes the gripper to set the stitch and opens it again afterwards. (C) $\boldsymbol{x}$ moves horizontally to pull the needle out of the tissue. (D) $state_g$ is reached, ASCOPE sets O_{tar} to $\boldsymbol{x}_{g_{n+1}}$ and activates `suture` SCT again.

Fig. 5: The instrument TCP $\boldsymbol{x}$ (displayed in red) moves along the corresponding spline s (blue). The legend in Fig. 5a depicts the selected LoA, DoSC, $f_c^{\parallel}$ and r_d, which is displayed in green.

of fluids from the stomach into the esophagus. During the procedure the top part of the stomach is wrapped around the esophageal sphincter located at the bottom of the esophagus. Then, a continuous suture is placed to hold the stomach in place [36].

Laparascopic suturing devices like the Covidien SILS Stich enable robotic suturing by designing a specialized drive unit allowing the attachment to an robotic arm as the MIRO [37]. This experiment focuses on placing multiple stitches with a real robotic suturing device mounted on a real MIRO as depicted in Fig. 1 and in the supplied video. The control over the opening and closing of the gripper, leading to the stitch placement, remains by the user at all times.

Hypothesis: When executing the `stitching` SCT multiple times, multiple continuous stitches are placed in the training pad allowing the autonomous placement of a continuous suture.

Experimental Design: The `stitching` SCT is executed with $O_{ref} = \boldsymbol{x}$. O_{tar} equals $\boldsymbol{x}_{g_n}$, $n \in [1, ..., 4]$. When reaching $state_g$, $\boldsymbol{x}_{g_{n+1}}$ is set and the `stitching` SCT is activated again.

Result: The sequence of stitches are successfully executed leading to a continuous suture. Fig. 5c depicts the movement of $\boldsymbol{x}$ during the experiment.

Discussion: This experiment shows that the presented method allows the placement of a continuous suture in L2.

V. Discussion and Conclusion

This work presents a novel method for teleoperated systems to provide haptic augmentation to the user during L1 and L2 while enabling continuous transitions between L0, L1, L2 and vice versa. Furthermore, the approach allows user interactions even in L2. Additionally, during L1 the degree of shared control, namely the level of support, can be varied according to the user's need.

During the execution of a task represented by an SCT, ASCOPE parameterizes VFs based on the selected LoA and the current context information. The presented iffVF enables haptic augmentation during L1 as well as autonomous movements during L2. The design of the iffVF takes the wrenches exerted on the input device into account which allows user interactions as acceleration and deceleration in L2. Additionally, it guarantees that the iffVF obeys other VFs like rVF as presented in [29]. The presented iffVF follows arbitrary splines allowing generalization to different tasks.

However, the splines as well as the SCT are currently hand designed by an expert. In the future, the design of SCT will be facilitated as in [38]. Finally, a user study will be conducted involving clinicians allowing the evaluation of the presented approach as well as its clinical relevance.

Acknowledgment

The Authors would like to gratefully acknowledge the financial support and endorsement from the DLR Management Board Young Research Group Leader Program and the Executive Board Member for Space Research and Technology.

References

[1] T. Haidegger, "Autonomy for Surgical Robots: Concepts and Paradigms," *IEEE Trans. Med. Robot. Bionics*, vol. 1, no. 2, pp. 65–76, May 2019.

[2] A. Attanasio, B. Scaglioni, M. Leonetti, A. F. Frangi, W. Cross, C. S. Biyani, and P. Valdastri, "Autonomous Tissue Retraction in Robotic Assisted Minimally Invasive Surgery – A Feasibility Study," *IEEE Robot. Autom. Lett.*, vol. 5, no. 4, pp. 6528–6535, Oct. 2020.

[3] P. Fiorini, K. Y. Goldberg, Y. Liu, and R. H. Taylor, "Concepts and Trends in Autonomy for Robot-Assisted Surgery," *Proc. IEEE*, vol. 110, no. 7, pp. 993–1011, Jul. 2022.

[4] G.-Z. Yang, J. Cambias, K. Cleary, E. Daimler, J. Drake, P. E. Dupont, N. Hata, P. Kazanzides, S. Martel, R. V. Patel *et al.*, "Medical robotics—regulatory, ethical, and legal considerations for increasing levels of autonomy," *Science Robotics*, vol. 2, no. 4, p. 8638, 2017.

[5] M. Stoiber, M. Pfanne, R. Strobl, Klaus H.and Triebel, and A. Albu-Schäffer, "Srt3d: A sparse region-based 3d object tracking approach for the real world." *International Journal of Computer Vision*, vol. 130, no. 4, pp. 1008–1030, 2022.

[6] M. Hwang, J. Ichnowski, B. Thananjeyan, D. Seita, S. Paradis, D. Fer, T. Low, and K. Goldberg, "Automating Surgical Peg Transfer: Calibration With Deep Learning Can Exceed Speed, Accuracy, and Consistency of Humans," *IEEE Trans. Automat. Sci. Eng.*, pp. 1–14, 2022.

[7] J. Rosen and J. Ma, "Autonomous Operation in Surgical Robotics," *Mechanical Engineering*, vol. 137, no. 09, pp. S15–S18, Sep. 2015.

[8] M. M. Rahman, M. V. Balakuntala, G. Gonzalez, M. Agarwal, U. Kaur, V. L. N. Venkatesh, N. Sanchez-Tamayo, Y. Xue, R. M. Voyles, V. Aggarwal, and J. Wachs, "SARTRES: a semi-autonomous robot teleoperation environment for surgery," *Computer Methods in Biomechanics and Biomedical Engineering: Imaging & Visualization*, vol. 9, no. 4, pp. 376–383, Jul. 2021.

[9] S. Sen, A. Garg, D. V. Gealy, S. McKinley, Y. Jen, and K. Goldberg, "Automating multi-throw multilateral surgical suturing with a mechanical needle guide and sequential convex optimization," in *2016 IEEE International Conference on Robotics and Automation (ICRA)*. Stockholm, Sweden: IEEE, May 2016, pp. 4178–4185.

[10] Hyosig Kang and J. Wen, "Autonomous suturing using minimally invasive surgical robots," in *Proceedings of the 2000. IEEE International Conference on Control Applications. Conference Proceedings (Cat. No.00CH37162)*. Anchorage, AK, USA: IEEE, 2000, pp. 742–747.

[11] S. A. Pedram, C. Shin, P. W. Ferguson, J. Ma, E. P. Dutson, and J. Rosen, "Autonomous Suturing Framework and Quantification Using a Cable-Driven Surgical Robot," *IEEE Trans. Robot.*, vol. 37, no. 2, pp. 404–417, Apr. 2021.

[12] M. Kam, H. Saeidi, M. H. Hsieh, J. U. Kang, and A. Krieger, "A Confidence-Based Supervised-Autonomous Control Strategy for Robotic Vaginal Cuff Closure," in *2021 IEEE International Conference on Robotics and Automation (ICRA)*. Xi'an, China: IEEE, May 2021, pp. 12 261–12 267.

[13] H. Saeidi, J. D. Opfermann, M. Kam, S. Wei, S. Leonard, M. H. Hsieh, J. U. Kang, and A. Krieger, "Autonomous robotic laparoscopic surgery for intestinal anastomosis," *Sci. Robot.*, vol. 7, no. 62, p. eabj2908, Jan. 2022.

[14] D. Zhang, B. Xiao, B. Huang, L. Zhang, J. Liu, and G.-Z. Yang, "A Self-Adaptive Motion Scaling Framework for Surgical Robot Remote Control," *IEEE Robot. Autom. Lett.*, vol. 4, no. 2, pp. 359–366, Apr. 2019.

[15] L. Rosenberg, "Virtual fixtures: Perceptual tools for telerobotic manipulation," in *Proceedings of IEEE Virtual Reality Annual International Symposium*. Seattle, WA, USA: IEEE, 1993, pp. 76–82.

[16] J. J. Abbott, P. Marayong, and A. M. Okamura, "Haptic Virtual Fixtures for Robot-Assisted Manipulation," in *Robotics Research*, S. Thrun, R. Brooks, and H. Durrant-Whyte, Eds. Berlin, Heidelberg: Springer Berlin Heidelberg, 2007, vol. 28, pp. 49–64, series Title: Springer Tracts in Advanced Robotics.

[17] S. A. Bowyer, B. L. Davies, and F. Rodriguez y Baena, "Active Constraints/Virtual Fixtures: A Survey," *IEEE Trans. Robot.*, vol. 30, no. 1, pp. 138–157, Feb. 2014.

[18] Z. Li, A. Gordon, T. Looi, J. Drake, C. Forrest, and R. H. Taylor, "Anatomical Mesh-Based Virtual Fixtures for Surgical Robots," *arXiv:2006.02415 [cs, eess]*, Jul. 2020, arXiv: 2006.02415.

[19] M. Muhlbauer, F. Steinmetz, F. Stulp, T. Hulin, and A. Albu-Schaffer, "Multi-Phase Multi-Modal Haptic Teleoperation," in *2022 IEEE/RSJ International Conference on Intelligent Robots and Systems (IROS)*. Kyoto, Japan: IEEE, Oct. 2022, pp. 7734–7741.

[20] M. S. Mühlbauer, F. Stulp, A. O. Albu-Schäffer, and J. Silvério, "Mixture of experts on riemannian manifolds for visual-servoing fixtures," in *2022 IEEE/RSJ International Conference on Intelligent Robots and Systems, Workshop on Probabilistic Robotics in the Age of Deep Learning*, 2022.

[21] M. Selvaggio, G. A. Fontanelli, F. Ficuciello, L. Villani, and B. Siciliano, "Passive Virtual Fixtures Adaptation in Minimally Invasive Robotic Surgery," *IEEE Robot. Autom. Lett.*, vol. 3, no. 4, pp. 3129–3136, Oct. 2018, number: 4.

[22] G. A. Fontanelli, G.-Z. Yang, and B. Siciliano, "A Comparison of Assistive Methods for Suturing in MIRS," in *2018 IEEE/RSJ International Conference on Intelligent Robots and Systems (IROS)*. Madrid: IEEE, Oct. 2018, pp. 4389–4395.

[23] H. Saeidi, J. D. Opfermann, M. Kam, S. Raghunathan, S. Leonard, and A. Krieger, "A Confidence-Based Shared Control Strategy for the Smart Tissue Autonomous Robot (STAR)," in *2018 IEEE/RSJ International Conference on Intelligent Robots and Systems (IROS)*, Oct. 2018, pp. 1268–1275, iSSN: 2153-0866.

[24] F. Ferraguti, N. Preda, G. De Rossi, M. Bonfe, R. Muradore, P. Fiorini, and C. Secchi, "A two-layer approach for shared control in semi-autonomous robotic surgery," in *2015 European Control Conference (ECC)*. Linz, Austria: IEEE, Jul. 2015, pp. 747–752.

[25] K. Shamaei, Y. Che, A. Murali, S. Sen, S. Patil, K. Goldberg, and A. M. Okamura, "A paced shared-control teleoperated architecture for supervised automation of multilateral surgical tasks," in *2015 IEEE/RSJ International Conference on Intelligent Robots and Systems (IROS)*. Hamburg, Germany: IEEE, Sep. 2015, pp. 1434–1439.

[26] R. Balachandran, H. Mishra, M. Cappelli, B. Weber, C. Secchi, C. Ott, and A. Albu-Schaeffer, "Adaptive authority allocation in shared control of robots using bayesian filters," in *2021 IEEE International Conference on Robotics and Automation (ICRA)*, 2020, pp. 11 298–11 304.

[27] S. Bustamante, G. Quere, K. Hagmann, X. Wu, P. Schmaus, J. Vogel, F. Stulp, and D. Leidner, "Toward Seamless Transitions Between Shared Control and Supervised Autonomy in Robotic Assistance," *IEEE Robot. Autom. Lett.*, vol. 6, no. 2, pp. 3833–3840, Apr. 2021.

[28] G. Quere, A. Hagengruber, M. Iskandar, S. Bustamante, D. Leidner, F. Stulp, and J. Vogel, "Shared Control Templates for Assistive Robotics," in *2020 IEEE International Conference on Robotics and Automation (ICRA)*, May 2020, pp. 1956–1962, iSSN: 2577-087X.

[29] K. Hagmann, A. Hellings-Kuß, J. Klodmann, R. Richter, F. Stulp, and D. Leidner, "A Digital Twin Approach for Contextual Assistance for Surgeons During Surgical Robotics Training," *Front. Robot. AI*, vol. 8, p. 735566, Sep. 2021.

[30] F. Dimension. "force dimension sigma.7". forcedimension.com. (accessed: 2024-01-24). [Online]. Available: https://www.forcedimension.com/products/sigma

[31] C. Schlenk, T. Bahls, S. Tarassenko, J. Klodmann, M. Bihler, and T. Wuesthoff, "Robot Integrated User Interface for Physical Interaction with the DLR MIRO in Versatile Medical Procedures," *J. Med. Robot. Res.*, vol. 03, no. 02, p. 1840006, Jun. 2018, number: 02.

[32] U. Seibold, K. Bernhard, T. Bahls, R. Haslinger, and F. Steidle, "THE DLR MIROSURGE SURGICAL ROBOTIC DEMONSTRATOR," in *The Encyclopedia of Medical Robotics*. Patel R, 2018, vol. Volume 1: Minimally Invasive Surgical RoboticsVolume, pp. 111–142.

[33] L. Grespan, P. Fiorini, and G. Colucci, *The Route to Patient Safety in Robotic Surgery*, ser. Springer Tracts in Advanced Robotics. Cham: Springer International Publishing, 2019, vol. 126.

[34] L. G. Ltd. "lübecker toolbox training exercises". luebeck-toolbox.com. (accessed: 2024-01-24). [Online]. Available: http://www.luebeck-toolbox.com/training.html

[35] M. Stoiber, M. Sundermeyer, and R. Triebel, "Iterative corresponding geometry: Fusing region and depth for highly efficient 3d tracking of textureless objects," in *Proceedings of the IEEE/CVF Conference on Computer Vision and Pattern Recognition (CVPR)*, June 2022, pp. 6855–6865.

[36] R. Nissen, "Gastropexy and "fundoplication" in surgical treatment of hiatal hernia," *The American journal of digestive diseases*, vol. 6, pp. 954–961, 1961.

[37] A. Kirst, A. Hellings-Kuß, K. Hagmann, M. Dyck, C. Schlenk, and J. Klodmann, "A novel end effector for telemanipulated suturing in robot-assisted laparoscopy," *Current Directions in Biomedical Engineering*, 2023.

[38] G. Quere, S. Bustamante, A. Hagengruber, J. Vogel, F. Steinmetz, and F. Stulp, "Learning and Interactive Design of Shared Control Templates," in *2021 IEEE/RSJ International Conference on Intelligent Robots and Systems (IROS)*. Prague, Czech Republic: IEEE, Sep. 2021, pp. 1887–1894.